Absolute thickness field measurement on curved axisymmetric thin free films with monochromatic light

J. Miguet, A. Bussonnière

Absolute thickness field measurement on curved axisymetric thin free films with monochromatic light

J. Miguet[1,2] and A. Bussonnière[2]
[1)]*Transfers, Interfaces and Processes (TIPs), Université Libre de Bruxelles, 1050, Brussels, Belgium*
[2)]*Matière et Systèmes Complexes, Univ. Paris Cité, CNRS, UMR 7057, 75013 Paris, France*

(*Electronic mail: adrien.bussonniere@u-paris.fr)

(Dated: 1 June 2024)

The thickness of thin films is a key parameter to understand their thinning dynamics and stability. Thickness measurements are commonly done using interferometry. White light illumination allows to measure the absolute thickness but is limited to small thicknesses ($< 2\mu$m) or is restricted to a point with a spectrometer. Monochromatic light gives access to a broader range of thicknesses but solely in a relative manner unless a reference thickness is known. These methods are extensively used to quantify thickness profiles of flat soap film. In contrast, they are applied on curved interfaces (bubble) only in few specific cases mainly due to the complexity arising from the curvature as the optical path depends on the position. In this paper, we elucidate the influence of the curvature and show that it can be used to measure the entire and absolute thickness profile using monochromatic light. We demonstrate the validity of the method on soap bubble, antibubble and catenoid soap films. This cost-effective technique is adapted to quantitatively study the thin film dynamics in these geometries.

INTRODUCTION

Free fluid films are defined by their high aspect ratio, with a transverse typical dimension, the thickness h, of order 100 nm – 10 µm and a typical size R of order 1 mm – 1 m[1–4]. These thin films are said to be free because no solid wall exists in the system *ie* when both surfaces connect the film to another fluid. Typical examples of such films are soap bubbles[5], flat liquid films[6], catenoids[7] or antibubbles[8]. All these objects undergo thinning through gravitationnal[9] and/or capillary-driven[3,10] drainage and may also exchange mass with their environment through their interfaces: typically in the form of evaporation for aqueous films[11] and dissolved gasses transfers for gas films[12]. This leads to the appearance of thinner, more fragile zones and utlimately to the nucleation of a hole[13,14] and the disapearance[15] of the thin film.

The dynamic thickness is therefore a key parameter to understand the lifetime and the stability of soap thin films[16,17]. As the typical thickness of such films is of the order of one micrometer, light interferes spontaneously inside the film resulting in the mesmerizing iridescence of these objects. This feature was used in visual arts, from painting[18] to photography[19] or performing arts[20]. The good understanding and modeling of the underlying physics has found a significant echo in numerical graphism as well[21,22].

The optical properties of thin films make interferometry methods the prime choice to precisely measure their thickness[23]. The different techniques can be sorted in two categories based on whether only one or several wavelengths are used to illuminate the film. When white light is used, absolute thicknesses can be assessed for relatively thin films $< 2\mu$m using a color matching with a color camera[24,25]. For thicker films the interference is lost as the camera channels (red, green and blue) are broadband spectrum detectors, such that interferences associated to each wavelength are mixed. To overcome this, spectrometers with a high spectral resolution can be used, allowing to measure thicknesses up to tens of µm[26]. However, such measurement are restricted to one point. Recently, costly hyperspectral cameras allowed to extend spectrometry measurements over a line[27] by diffracting the light through a slit, or over an area by placing band-pass filters on each pixel of a camera sensor[28]. In both cases, there is still strong restrictions in the spatial and/or spectral resolution.

Alternatively, monochromatic illumination avoids color mixing. Coupled with a camera, it enables high resolution mapping of the thickness *variation* field. Thickness, in this case, is relative as the orders of interference of the fringes are *a priori* unknown. A reference in the thickness field is then necessary to reconstruct the profile, for example the black film which gives the 0th order and therefore a thickness reference. Most of these technique are applied in reflection to improve the contrast and are therefore mainly restricted to flat films[29] or large bubbles[30], for which a large area is detected. In the case of curved interfaces, such as soap bubbles, these techniques are used in transmission but only few studies were performed in such configuration due to the complications induced by the curvature (variation of the incident angle)[9,31,32].

In this paper, we use of an analytical trick to measure the complete and absolute thickness profile of curved objects with monochromatic transmitted light. The method applies on light-transmitting films *ie* not on metallic thin films broadly used for coating purposes. The main idea of the method can be summarized as follows, from a typical interference pattern observed with collimated light as is shown in figure 1b). This pattern is axisymetric with respect do the vertical line that passes through the center of the bubble. In addition, the fringes are bended, such that if we draw a horizontal line on the bubble, we can identify maxima and minima of intensity associated with constructive and destructive fringes. The two possible contributions to the phase change are the variation of the thickness and of the angle of incidence of the incoming light due to the curvature. The basic laws of optics pro-

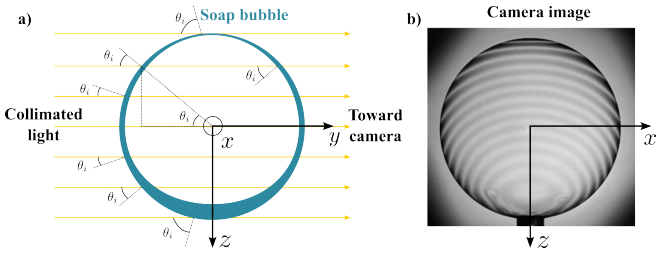

FIG. 1. a) Schematic of the collimated monochromatic light paths through a soap bubble. b) Typical image obtained on the camera for a stratified soap bubble.

vide one equation on the thickness h for each fringe, where the influence of the incident angle is easily obtained from the position on the sphere. Assuming that the thickness profile is axisymetric, like the interference pattern, we can cast different guesses on the absolute order of interference until all maxima and minima provide a consistent, *ie* equal, value for h. This illustrative explanation is extended to the whole interference pattern and is valid in principle for any curved, axisymetric, free film for which the incident angle can be computed from the position, as shown in the following. This relatively low-cost technique (monochromatic light + camera) is easy to use (fringe detection). It paves the way towards precise free film dynamic studies on curved interfaces.

I. OPTICAL INTERFERENCE ON CURVED FREE FILMS

A typical experiment consists in illuminating a soap bubble with a collimated monochromatic light (sodium-vapor lamp with $\lambda = 589$ nm) and to record the transmitted interference pattern generated, see figure 1. All free films in this study are obtained with the commercial dishwashing liquid Dreft by Proctor and Gamble. The soap bubble has slowly drained resulting in a thickness stratification in the z direction with an axisymmetric profile. As shown in figure 1 b) the interference pattern differs from a flat soap film where horizontal fringes are expected[29]. The observed curvature of the fringes is due to a change in the incident angle of the collimated incoming light, resulting in an optical path difference that varies with the position on the bubble.

To explicit this dependence, let us consider a free film of thickness h with an optical index n_2 inside a media of optical index n_1 as shown in figure 2. An incident ray having an incident angle θ_i will be partly transmitted directly and some part of it will be reflected, potentially several times. Interference then occurs between the directly transmitted ray and those which are reflected an even number of times inside the free film. The optical path difference Δ between the first ray and the one that is reflected twice in the free film is expressed as $\Delta = n_2(|BC|+|CD|) - n_1|BE| = 2n_2|AB| - n_1|BE|$, where the vertical bars denote the length of the corresponding segment. Simple geometric calculation gives $|AB| = h/\cos\theta_t$, where θ_t is the angle of the transmitted ray in the free film with respect to the horizontal. Using Snell-Descartes law we obtain

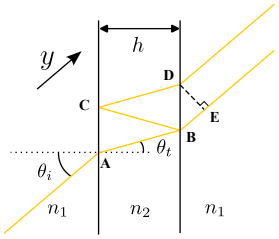

FIG. 2. Schematic of the light inteference inside a free fluid film.

$|AB| = h/\sqrt{1-(n_1\sin\theta_i/n_2)^2}$. Similarly, we obtain $|BE| = |BD|\cos(\pi/2-\theta_t) = |BD|\sin\theta_i$ and $|BD| = 2|AB|\sin\theta_t = 2|AB|n_1\sin\theta_i/n_2$. Finally the optical path difference is expressed as:

$$\Delta(\theta_i) = 2n_2 h\sqrt{1-\left(\frac{n_1}{n_2}\sin\theta_i\right)^2} = hg(\theta_i), \qquad (1)$$

where we have separated the contribution of the thickness h and that of the curvature $g(\theta_i)$ to the optical path difference.

II. BUBBLE

We first derive the principles of the method on a bubble and demonstrate its validity with an independent measurement.

Classically, for a flat interface, the optical path difference only depends on the thickness as the incident angle is fixed and interference fringes are associated to a unique thickness. For curved interfaces, θ_i is not constant and the fringes are not associated to a fixed thickness, which is the key phenomenon, together with axisymmetry, to determine the full thickness profile. For a soap bubble the incident angle corresponds to the angle between the normal vector $\vec{n}$ and incident direction $\vec{y}$ so $\cos\theta_i = |\vec{y}.\vec{n}| = |y|/R$, see figure 1 a). Using the sphere equation, the incident angle evolution with the position is given by:

$$\cos\theta_i = \frac{|y|}{R} = \sqrt{1-\frac{x^2+z^2}{R^2}}, \qquad (2)$$

and the curvature function defined in Eq. (1) becomes for the specific case of a soap bubble ($n_1 = 1$ and $n_2 = n_w$ with n_w the optical index of water) :

$$g^b(x,z) = 2n_w\sqrt{1-\frac{1-\cos^2\theta_i}{n_w^2}} = 2n_w\sqrt{1-\frac{x^2+z^2}{n_w^2R^2}}. \qquad (3)$$

The incident angle also has an influence on the reflection and transmission coefficients as can be seen on the image in figure 1 b) where a higher contrast is observed on the bubble edge. For a randomly polarized light, in the general case, the reflection coefficient $\mathscr{R}$ is given by the Fresnel coefficients:

$$\begin{aligned}\mathscr{R} &= \frac{1}{2}(\mathscr{R}_\perp + \mathscr{R}_\parallel)\\ &= \frac{1}{2}\left(\frac{n_1\cos\theta_i - n_2\cos\theta_t}{n_1\cos\theta_i + n_2\cos\theta_t}\right)^2 + \frac{1}{2}\left(\frac{n_2\cos\theta_i - n_1\cos\theta_t}{n_2\cos\theta_i + n_1\cos\theta_t}\right)^2,\end{aligned} \qquad (4)$$

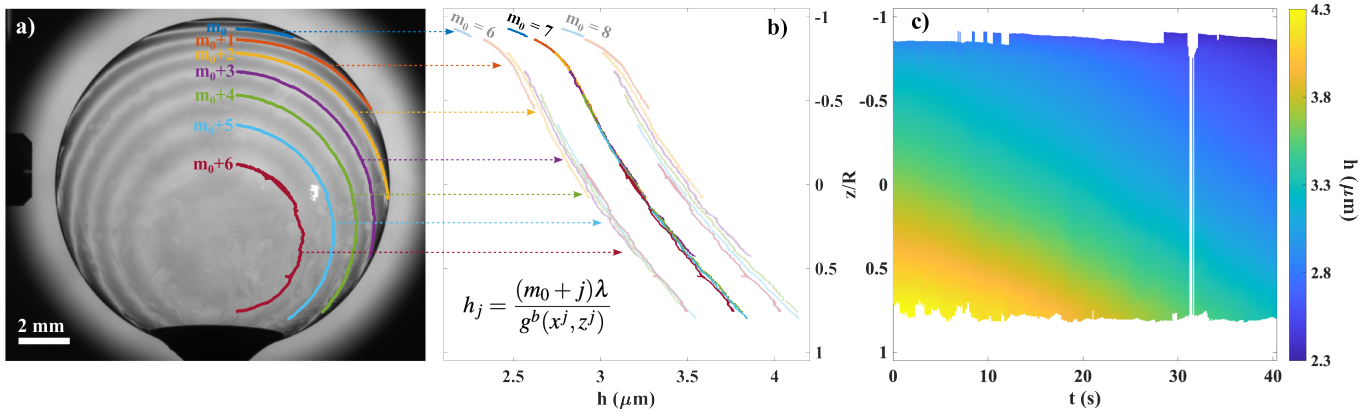

FIG. 3. a) Image of a soap bubble backlighted with monochromatic light showing the different constructive fringes and their respective assigned order. b) Thickness evolution as a function of the altitude associated to each fringes (same color as in a)) for different m_0 guesses. c) Thickness profiles over time (10 FPS) measured using the technique..

with $\mathscr{R}_\perp$ and $\mathscr{R}_\parallel$ the reflection coefficient for perpendicularly (resp. parallelly) polarized light. Eq. 4 shows that $\mathscr{R}$ increases with the incident angle, which is associated to a decrease of the transmission since $\mathscr{T}+\mathscr{R}=1$, where $\mathscr{T}$ is the transmission coefficient. This results in destructive interference fringes becoming darker for high θ_i (close the object edges) in agreement with the observation in figure 1 b). Combining the effects of the curvature on the reflection coefficients and on the optical path, and considering the multiple reflections, the intensity transmitted after one free film is given by[33]:

$$I_t(\theta_i) = \frac{I_0}{1+\mathscr{F}(\theta_i)\sin^2\frac{\delta(\theta_i)}{2}}, \tag{5}$$

with I_0 the incident intensity, $\mathscr{F}(\theta_i) = 4\mathscr{R}(\theta_i)/(1-\mathscr{R}(\theta_i))^2$ and $\delta(\theta_i) = 2\pi\Delta(\theta_i)/\lambda$ the phase difference associated to the optical path difference. For the objects considered here, the light rays cross two free films. The light intensity received by the second interface is given by equation (5) and the total intensity received by the camera I_T, if the two films have the same thickness, is:

$$I_T(\theta_i) = \frac{I_t}{1+\mathscr{F}(\theta_i)\sin^2\frac{\delta(\theta_i)}{2}} = \frac{I_0}{\left(1+\mathscr{F}(\theta_i)\sin^2\frac{\delta(\theta_i)}{2}\right)^2}. \tag{6}$$

Note that the local maxima and minima corresponding to the center of the fringes are the same for Eqs. (5) and (6), meaning that the presence of a second film does not affect the position of the fringes; it however improves the contrast. The intensity ranges from $I_0/(1+\mathscr{F}(\theta_i))^2$ (destructive interference) to I_0 (constructive) so the contrast between fringes evolves with the incident angle. For image analysis purposes, the operation $1+(I_T/I_0-1)/[1-1/(1+\mathscr{F}(\theta_i))^2]$ allows to make the contrast uniform over the image.

The relation between the measured intensity and the thickness is now explicitly given; however it cannot be inverted directly due to the sinus function. We now show that the curvature of the interface can nevertheless be used to extract the interference order without the knowledge of a reference thickness or of the 0-order interference, as opposite to flat interfaces.

For the sake of clarity, let us first describe the relation between a constructive fringe at incident angle θ_i^m and order of interference m (*a priori* unknown) and its immediate neighbor *on the same horizontal line* (*ie* same thickness), at incident angle θ_i^{m+1} and order of interference $m+1$. We then have $\delta_m(\theta_i^m) = 2\pi h g(\theta_i^m)/\lambda = 2m\pi$ and the thickness is $h = m\lambda/g(\theta_i^m)$ for the m-order fringe and $h = (m+1)\lambda/g(\theta_i^{m+1})$ for the (m+1)-order fringe. Since the thickness is the same the interference order can then be deduced and is equal to $m = g(\theta_i^m)/(g(\theta_i^{m+1}) - g(\theta_i^m))$ giving the absolute thickness.

This method can be extended over all the fringes and therefore over the entire profile. As shown in figure 3 a), the position of the constructive fringes are first extracted. The unknown order m_0 is allocated to the top fringe and the consecutive ones are assigned with the order m_0+j for the j-th fringe. For each constructive interference, the corresponding thickness $h_j = (m_0+j)\lambda/g^b(x^j,z^j)$ is plotted as a function of z using eq. (3). Figure 3 b) shows the results for different m_0 guesses. Note that the different colors correspond to the different fringes labeled in figure 3 a). Only the right-hand part of the fringes are shown on the figure but the entire fringes were used in figure 3 b). We can first see that for a given fringe all the points collapse on a single curve, indicating that the pattern is indeed axisymetric and then the thickness too.

The different fringes collapse together for only one m_0, here $m_0 = 7$. The guess for $m_0 = 6$ and 8 are also shown to illustrate the sensitivity of the method to the m_0 guesses. Once the order of interference is known, we see that a given fringe provides a measure of the thickness *profile* over its whole vertical extent along the sphere, contrary to the flat film case. Combining the different fringes therefore gives access to the entire thickness field as shown in figure 3 b). Finally by repeating this step for the different images of a time serie, the entire thickness profile evolution can be extracted as shown in figure 3 c).

To validate the technique, a fiber spectrometer (Ocean Optics USB 2000+), visible on the left of figure 3 a) is synchronized with the camera. The spectrometer signal

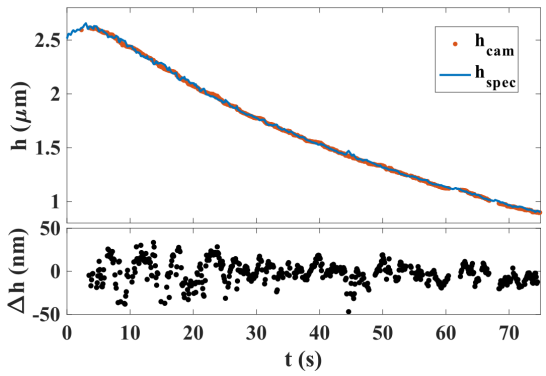

FIG. 4. (top) Comparison between the thicknesses h_{spec} measured by the spectrometer and h_{cam} measured by the technique presented here, as a function of time. (bottom) Thickness difference between the two methods.

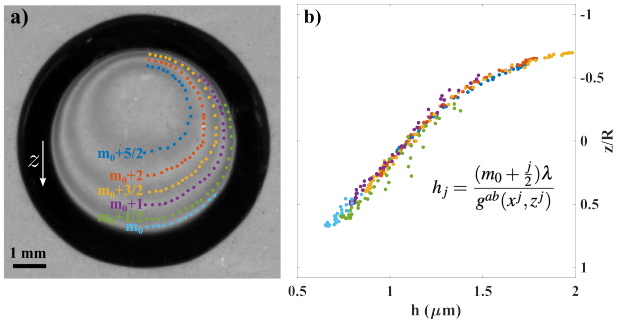

FIG. 5. a) Image of an antibubble showing the interference pattern induced by the thin air film. b) Thickness profile corresponding to image a) with $m_0 = 1$. The colors are associated to the different fringes marked in a).

is analysed with a home-made Matlab code. After a normalisation by the light reference spectrum, a first rough estimate of the thickness is obtained, using a Fourier transform. The maxima and minima are then extracted and arranged in vectors corresponding respectively to λ_M and λ_m. Recalling the theoretical formula of normal incidence interference $I \sim 1 - \cos(4\pi n_w h/\lambda)$ we see that maxima (resp. minima) occur when $2nh/\lambda_M + 1/2$ (resp. $2nh/\lambda_m$) are integers. A refinement of the thickness is then performed over a thickness window surrounding the rough estimation by minimising the function: $\sum_{i=1}^{N_M}(|[\frac{2nh}{\lambda_M(i)}+\frac{1}{2}]-(\frac{2nh}{\lambda_M(i)}+\frac{1}{2})|)+\sum_{i=1}^{N_m}|([\frac{2nh}{\lambda_m(i)}]-\frac{2nh}{\lambda_m(i)}|)$, where $[.]$ is the round function, and N_M (resp. N_m) the number of maxima (resp. minima).

The resulting thickness extracted from the spectrometer, corresponding to the thickness at the middle of the bubble is compared to the one measured with the fringe analysis in figure 4. A remarkable agreement is found between the two techniques with a difference between the methods always less than 50 nm, corresponding to a relative error of 2%, as shown in the bottom curve of figure 4. The error between the methods can mainly be ascribed to the image noise and thickness recirculation (marginal regeneration[34], visible in figure 3 a)) in the free film disturbing the spectrometer measurement. Note that some thickness measurements with the camera are missing, especially at the beginning of the experiment, due to the difficulty to fully automatize the image analysis.

We now show that this method can be applied in principle to any curved interfaces for which the function $g(\theta_i)$ can be calculated with antibubbles as a first example.

III. ANTIBUBBLE

Antibubbles, see figure 5 a), correspond to a spherical thin air film sandwiched between a soapy droplet and a soapy bulk, a situation opposite to classical soap bubbles. In this case, the antibubble is obtained by releasing a jet with a straw filled with a solution of Dreft and about 5 % of glycerol. Some glycerol is initially deposited at the bottom of the fresh Dreft solution in which the antibubble is made, in order to obtain a 'levitating' antibubble within the bath[8,35]. The black corona around the object corresponds to the area where the light is totally reflected at the water-air interface (for $\theta_i > 48.6^o$). For an antibubble the relation g between the position inside the accessible region ($\theta_i < 48.6^o$) and the incident angle becomes:

$$g^{ab}(x,z) = 2\sqrt{1 - n_w^2 \frac{x^2+z^2}{R^2}}. \tag{7}$$

Here both constructive and destructive fringes were used and were identified by hand clicking, see figure 5 a). Destructive fringes correspond to $\delta = (2m+1)\pi$ with m an integer. In this more general case, the reference order m_0 (constructive) or $m_0 + \frac{1}{2}$ (destructive) is attributed to the fringe corresponding to the thinnest portion of the film, based on physical considerations. Then, the successive fringes are sorted with the index j, starting from 1, and their order of interference is $m_0 + \frac{j}{2}(+\frac{1}{2})$ as all fringes are analysed. The $(+\frac{1}{2})$ must be accounted for if the first fringe is destructive.

In the case of the antibubble analysed in figure 5a, the hydrostatic pressure being higher at the bottom than at the top, the gas film drains upward and the thickness is therefore thinner at the bottom[36]. The smallest order m_0 is then attributed to the bottom one (in cyan) as it corresponds to a constructive interference. If the first interference had been destructive $m_0 + 1/2$ would have been used. The collapse of the fringes is obtained for $m_0 = 1$ as shown in figure 5 b). This example shows the simplicity and the efficiency of this method to extract thickness profiles. Note that we assumed here the gradient direction (thinner film at the bottom) to attribute the fringes orders. Nonetheless if the order of the fringes is not correctly attributed, increasing order from top to bottom, no collapse of the fringes can be obtained so the gradient direction is not required.

IV. CATENOID

The method has been illustrated on spherical objects, we now demonstrate its versatility by considering a catenoid as

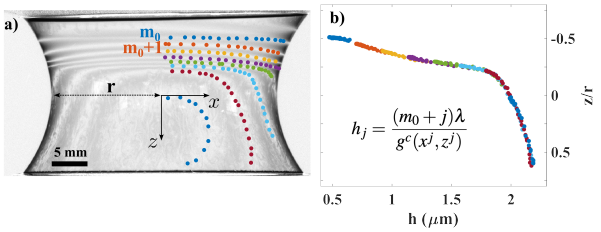

FIG. 6. a) Image of a catenoid backlighted with monochromatic light showing the peculiar interference pattern. b) Thickness profile corresponding to the image a) with m_0=1. The colors are associated to the different fringes marked in a).

shown in figure 6. Two 3D printed circles were mounted on a post. The circles are soaked in the soapy solution while being in contact and are then slowly moved apart resulting in the formation of a catenoid. To express the function g we consider a catenoid of small radius r. In the cartesian coordinate system shown in figure 6 a) the surface equation is given by $F = x^2 + y^2 - r^2\cosh^2(z/r) = 0$[37]. The incident angle is then given by $\cos\theta_i = |\vec{y}.\vec{n}|$, with $\vec{n} = \vec{\nabla}F/||\vec{\nabla}F||$. After straightforward calculations, the function g^c for a catenoid and a given point in the plan (x,z) is given by:

$$g^c(x,z) = 2n_w\sqrt{1 - \frac{1}{n_w^2} + \frac{r^2\cosh^2\left(\frac{z}{r}\right) - x^2}{n_w^2 r^2\cosh^4\left(\frac{z}{r}\right)}}. \qquad (8)$$

Figure 6 a) shows the peculiar interference pattern generated by a catenoid. We identify the different constructive fringes and then apply the same method to find the first order m_0. The different fringes collapse in this case for $m_0 = 1$ and the corresponding thickness profile is shown in figure 6 b). The thicknesses calculated for the different fringes feature an excellent overlap and therefore the overall coherence of the profile is demonstrated.

V. DISCUSSION

We now turn to the different limitations of the technique. As invoked earlier one of the strongest restrictions of the method is that the thickness of the front and rear films has to be the same for a clear interference pattern to occur. However, this conditions is not too restrictive in the case of soap films subjected to gravity. Another limitation is the ability to properly count the fringes. If a fringe is missed then no collapse or only partial collapse will be achieved. This again is not too restrictive when interference are hand-clicked but greatly complicates an automated image analysis. Finally, the different examples shown exhibit monotonic, stratified, thickness fields which depend solely on z. However, the method should still hold even for non-monotonic field functions of both x and z as long as the fringes orders can be accurately attributed: once m_0 is chosen the other fringes order needs to be defined with respect to it. Indeed, the axisymmetry of the system is a sufficient but not a necessary condition. In the case where two free films are crossed by the lights beams, the necessary condition for Eq. (6) to hold is a mirror symmetry *ie* an orthogonal symmetry of the free film with respect to the plan parallel to the camera sensor that passes through the geometrical center of the considered object. In this case, a varying thickness along the axis x also yields a unique interference pattern for a unique thickness profile. A more detailed study of the accessible profiles would be required to clarify these conditions but is out of the scope of this paper. Note that the method still holds for uniform thickness fields.

The temporal resolution of the measurements is essentially limited by (i) the frame rate of the camera (ii) the image intensity *ie* the combination of aperture, sensibility of the sensor, exposure time and lens properties, as well as the source intensity. These parameters should be tuned according to the physical system studied.

The size of the systems that can be studied is essentially slaved to (i) the spatial resolution, so that fringes can be properly distinguished (ii) the optical depth that should not limit the neat caracterization of the interference figure (iii) the curvature of the film that should be large enough for the fringes to be curved. While the first point may provide a lower limit for the size af accessible systems, the last two are the constraints for the largest ones. A complete determination of these limits is beyond our scope.

CONCLUSION

In conclusion, we propose a simple and cost-effective technique to measure absolute thickness maps on curved interfaces with monochromatic light, without the need of a reference thickness. This method is based on the coupled dependence of the phase difference with the thickness and the angle of incidence *ie* the position on the object. The technique can be summarized in the following steps:

1. Extract the position of the different fringes
2. Choose the order of the first fringe m_0 and attribute the other orders with respect to m_0
3. Plot the thickness associated to each fringe using $h_j = (m_0 + j)\lambda/g(x,z)$ for different m_0 guesses.
4. Choose the m_0 that allows collapsing the calculated thicknesses

The second step might require physical consideration as done here with gravitational drainage. If no fringes arrangement can be inferred, several ordering can be assumed and steps 2. to 4. can be repeated until fringes collapse is achieved. Note that in this summary we assumed that only constructive fringes are used. If one considered destructive fringes the fringe order are half-integer as described for the anti-bubble case.

The proposed method provides a new tool to quantitatively probe the stability and dynamic of curved soap films where

the geometrical extension/contraction of a draining film element might trigger different behaviors as those observed in flat films. In addition to slow draining films, this technique could be used to study faster dynamics such as in drops/bubbles coalescence or during the formation of antibubbles where such peculiar interference patterns have been observed[38]. Only air-water interfaces were probed here but the method still holds for systems involving phases with different optical indexes and could also be used in fields such as double emulsions.

Finally, one can imagine extending this approach to flat films by using a pair of lenses similar to the setup used in Haidinger fringes[39]. The idea is then to curve the light instead of the interface and then to collimate it back towards the camera. This extension is less restrictive as only one thin film is probed so no symmetry is required. Moreover, by tuning the lens focal length, one could characterize films with thicknesses ranging from few hundreds of nanometers to hundreds micrometers opening a new avenue to measure thin films in a more general context such as in film coating.

SUPPLEMENTARY MATERIAL

The matlab code used to analyse the images automatically is provided in the supplementary material. Note that this code is experiment-dependant as some absolute threshold has been used nonetheless this code may serve as a basis for readers interested in this method.

ACKNOWLEDGMENTS

JM thanks Mairie de Paris, Emergence Program for funding. For the purpose of Open Access, a CC-BY public copyright licence has been applied by the authors to the present document and will be applied to all subsequent versions up to the Author Accepted Manuscript arising from this submission.

DATA AVAILABILITY STATEMENT

The videos that support the findings of this study are available from the corresponding author upon reasonable request. The maltab code used to analysed the images is provided in the supplementary material.

[1] N. Pagureva, S. Tcholakova, K. Rusanova, N. Denkov, and T. Dimitrova, "Factors affecting the coalescence stability of microbubbles," Colloids and Surfaces A: Physicochemical and Engineering Aspects **508**, 21–29 (2016).
[2] B. Scheid, S. Dorbolo, L. R. Arriaga, and E. Rio, "Antibubble dynamics: the drainage of an air film with viscous interfaces," Physical review letters **109**, 264502 (2012).
[3] H. Lhuissier and E. Villermaux, "Bursting bubble aerosols," J. Fluid Mech. **696**, 5–44 (2012).
[4] C. Cohen, B. Darbois Texier, E. Reyssat, J. H. Snoeijer, D. Quéré, and C. Clanet, "On the shape of giant soap bubbles," Proceedings of the National Academy of Sciences **114**, 2515–2519 (2017).
[5] C. V. Boys, *Soap bubbles, their colours and the forces which mold them*, Vol. 542 (Courier Corporation, 1959).
[6] K. Mysels, S. Frankel, and K. Shinoda, *Soap films: studies of their thinning and a bibliography* (Pergamon Press, 1959).
[7] T. H. Colding and W. P. Minicozzi, "Shapes of embedded minimal surfaces," Proceedings of the National Academy of Sciences **103**, 11106–11111 (2006).
[8] Y. Vitry, S. Dorbolo, J. Vermant, and B. Scheid, "Controlling the lifetime of antibubbles," Advances in colloid and interface science **270**, 73–86 (2019).
[9] G. d. Debrégeas, P.-G. De Gennes, and F. Brochard-Wyart, "The life and death of" bare" viscous bubbles," Science **279**, 1704–1707 (1998).
[10] J. Miguet, M. Pasquet, F. Rouyer, Y. Fang, and E. Rio, "Stability of big surface bubbles: impact of evaporation and bubble size," Soft Matter **16**, 1082–1090 (2020).
[11] L. Champougny, J. Miguet, R. Henaff, F. Restagno, F. Boulogne, and E. Rio, "Influence of evaporation on soap film rupture," Langmuir **34**, 3221–3227 (2018).
[12] B. Scheid, J. Zawala, and S. Dorbolo, "Gas dissolution in antibubble dynamics," Soft Matter **10**, 7096–7102 (2014).
[13] S. Poulain, E. Villermaux, and L. Bourouiba, "Ageing and burst of surface bubbles," Journal of fluid mechanics **851**, 636–671 (2018).
[14] E. Chatzigiannakis and J. Vermant, "Breakup of thin liquid films: From stochastic to deterministic," Physical review letters **125**, 158001 (2020).
[15] S. Tobin, A. Meagher, B. Bulfin, M. Möbius, and S. Hutzler, "A public study of the lifetime distribution of soap films," American Journal of Physics **79**, 819–824 (2011).
[16] S. K. Mysels K. J. and F. S., *Soap Films, Studies of Their Thinning and a Bibliography* (Pergamon, 1959).
[17] I. Cantat, S. Cohen-Addad, F. Elias, F. Graner, R. Höhler, O. Pitois, F. Rouyer, and A. Saint-Jalmes, *Foams: structure and dynamics* (OUP Oxford, 2013).
[18] F. Behroozi, "Soap bubbles in paintings: Art and science," American Journal of Physics **76**, 1087–1091 (2008).
[19] See for example this collaborative work with picture from Serge Guichard: https://www.slashbubblesparis.com/collaborations?lightbox=dataItem-ld3dkbbj13.
[20] P.-Y. Fusier, F. Graner, F. Restagno, E. Rio, U. Shoaib, and O. Vallet, "Faire des bulles, tout un art, toute une science," Reflets de la physique , 31–33 (2020).
[21] B. E. Smits and G. W. Meyer, "Newton's colors: simulating interference phenomena in realistic image synthesis," in *Photorealism in Computer Graphics* (Springer, 1992) pp. 185–194.
[22] W. Huang, J. Iseringhausen, T. Kneiphof, Z. Qu, C. Jiang, and M. B. Hullin, "Chemomechanical simulation of soap film flow on spherical bubbles," ACM Transactions on Graphics (TOG) **39**, 41–1 (2020).
[23] S. P. Frankel and K. J. Mysels, "Simplified theory of reflectometric thickness measurement of structured soap and related films," Journal of Applied Physics **37**, 3725–3728 (1966).
[24] K. Kitagawa, "Thin-film thickness profile measurement by three-wavelength interference color analysis," Applied optics **52**, 1998–2007 (2013).
[25] J. M. Frostad, D. Tammaro, L. Santollani, S. B. de Araujo, and G. G. Fuller, "Dynamic fluid-film interferometry as a predictor of bulk foam properties," Soft Matter **12**, 9266–9279 (2016).
[26] J. Delacotte, L. Montel, F. Restagno, B. Scheid, B. Dollet, H. A. Stone, D. Langevin, and E. Rio, "Plate coating: influence of concentrated surfactants on the film thickness," Langmuir **28**, 3821–3830 (2012).
[27] A. Bussonnière and I. Cantat, "Local origin of the visco-elasticity of a millimetric elementary foam," Journal of Fluid Mechanics **922**, A25 (2021).
[28] V. Chandran Suja, J. Sentmanat, G. Hofmann, C. Scales, and G. G. Fuller, "Hyperspectral imaging for dynamic thin film interferometry," Scientific reports **10**, 11378 (2020).
[29] V. A. Nierstrasz and G. Frens, "Marginal regeneration in thin vertical liquid films," Journal of colloid and interface science **207**, 209–217 (1998).
[30] H. Kočárková, F. Rouyer, and F. Pigeonneau, "Film drainage of viscous liquid on top of bare bubble: Influence of the bond number," Phys. Fluids **25** (2013).
[31] C. Bartlett, A. T. Oratis, M. Santin, and J. C. Bird, "Universal non-monotonic drainage in large bare viscous bubbles," Nat. Commun. **14**, 877 (2023).
[32] A. Bussonnière, A. Antkowiak, F. Ollivier, M. Baudoin, and R. Wunenburger, "Acoustic sensing of forces driving fast capillary flows," Physical Review Letters **124**, 084502 (2020).

[33]M. BORN and E. WOLF, "Chapter vii - elements of the theory of interference and interferometers," in *Principles of Optics (Sixth Edition)*, edited by M. BORN and E. WOLF (Pergamon, 1980) sixth edition ed., pp. 256–369.
[34]J. Miguet, M. Pasquet, F. Rouyer, Y. Fang, and E. Rio, "Marginal regeneration-induced drainage of surface bubbles," Physical Review Fluids **6**, L101601 (2021).
[35]W. Suhr, "Gaining insight into antibubbles via frustrated total internal reflection," European journal of physics **33**, 443 (2012).
[36]S. Dorbolo, E. Reyssat, N. Vandewalle, and D. Quéré, "Aging of an antibubble," Europhysics Letters **69**, 966 (2005).
[37]M. Ito and T. Sato, "In situ observation of a soap-film catenoid—a simple educational physics experiment," European Journal of Physics **31**, 357 (2010).
[38]D. Beilharz, A. Guyon, E. Li, M.-J. Thoraval, and S. T. Thoroddsen, "Antibubbles and fine cylindrical sheets of air," Journal of fluid mechanics **779**, 87–115 (2015).
[39]J.-A. Kim, J. W. Kim, C.-S. Kang, J. Jin, and J. Y. Lee, "An interferometric system for measuring thickness of parallel glass plates without 2π ambiguity using phase analysis of quadrature haidinger fringes," Review of Scientific Instruments **88** (2017).